A π-Donor Spectrochemical Series for X in $(Me_5C_5)_2TiX$, and β-Agostic Interactions in X = Et and N(Me)Ph

Wayne W. Lukens, Jr., Milton R. Smith III, and Richard A. Andersen*

Contribution from the Department of Chemistry, Chemical Sciences Division, Lawrence Berkeley Laboratory, University of California, Berkeley, California 94720

Received September 25, 1995[⊗]

Abstract: The EPR and electronic spectra of d^1-bent metallocene compounds of the type Cp^*_2TiX, where X is halide, alkoxide, amide, alkyl, or hydride and $Cp^* = Me_5C_5$, have been studied. Several of these compounds are new, and those with X = N(Me)H and F were characterized by X-ray crystallography. The crystal structure of $Cp^*_2TiN(Me)H$ showed that the N(Me)H ligand lies on the plane defined by Cp*(centroid)−Ti−Cp*(centroid). This is the sterically most unfavorable conformation but allows maximum Ti−N π-bonding. The anisotropic frozen solution EPR spectra were analyzed by the method used by Petersen and Dahl for the d^1-metallocenes, Cp_2VX_2, which gives g_x, g_y, and g_z. Although the values of g_x and g_z are relatively constant throughout the series, the value of g_y varies with the π-donor ability of X. The π-donor series is N(Me)H ≈ NH_2 ≈ OMe > OPh ≈ F > N(Me)Ph > Cl > Br > I > H. Among the known alkyls, the π-donor ability was Et > Me > *n*-Pr ≈ CH_2CMe_3 > $CH_2C_6H_5$, which is rationalized, in part, by a β-agostic interaction in the case of Et. The β-agostic interaction in Cp^*_2TiEt and in $Cp^*_2TiN(Me)Ph$ was investigated by variable-temperature EPR spectroscopy giving an enthalpy and entropy for the agostic interaction. For Cp^*_2TiEt the parameters for the agostic interaction are $\Delta H° = -1.93(3)$ kcal/mol and $\Delta S° = -6.3(2)$ eu, and for $Cp^*_2TiN(Me)Ph$, $\Delta H° = -1.5(1)$ kcal/mol and $\Delta S° = -7.9(5)$ eu.

Introduction

Cp^*_2TiX complexes (X is a monodentate, one-electron ligand such as a halide, amide, alkoxide, or alkyl group and Cp* is Me_5C_5) appear to be ideal for the study of ligand-to-metal π-bonding. They are monomeric, unlike $[Cp_2TiX]_2$ in which the electrons are coupled. They have a single electron in the a_1 orbital making electronic spectroscopy simple, unlike Cp_2VX in which the a_1 and b_2 orbitals are singly occupied.[1−3] The trivalent decamethyltitanocenes have an empty b_2 orbital available for π-bonding, unlike Cp_2MX_2 in which the b_2 orbital is used for σ-bonding.

The best known bonding model for bent metallocenes is due to Lauher−Hoffmann; Figure 1 shows the metallocene orbitals with two different coordinate systems.[4−9] The coordinate system used here, due to Petersen and Dahl, is more convenient because this coordinate system minimizes the mixing the d_{z^2} and $d_{x^2-y^2}$ orbitals.[10,11] This metallocene bonding model is supported by the work of Petersen and Dahl in which single-crystal EPR spectroscopy shows that the single electron in $(\eta^5\text{-}MeC_5H_4)_2VCl_2$ and Cp_2VS_5 occupies an orbital that is perpendicular to the plane formed by the metal and the two Cp centroids and is largely of d_{z^2} parentage (in this coordinate system).[10,11] In Cp^*_2TiX, the unpaired electron resides in the low-lying a_1 orbital which is largely d_{z^2}. The empty b_2 orbital can interaction with the p_z orbital of the X ligand to form a π-bond and a π-antibond; the latter is the b_2 orbital. Thus, the energy of the $1a_1 \rightarrow b_2$ transition depends directly upon the

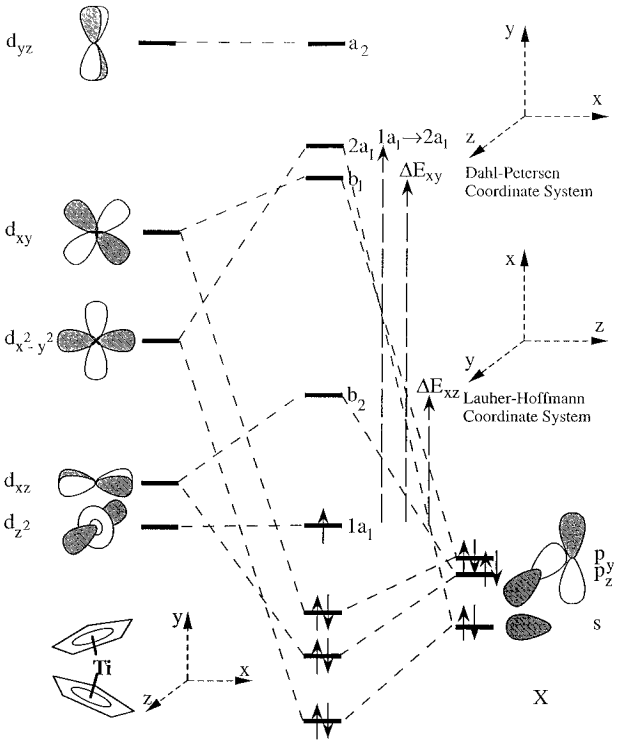

Figure 1. Qualitative MO diagram for a bent metallocene (after Lauher and Hoffmann).[4] The broken arrows labeled $1a_1 \rightarrow 2a_1$, ΔE_{xy}, and ΔE_{xz} show the observed transitions.

* Address correspondence to this author at the Department of Chemistry.
⊗ Abstract published in *Advance ACS Abstracts,* January 15, 1996.

(1) Green, J. C.; Payne, M. P.; Teuben, J. H. *Organometallics* **1983**, *2*, 203−210.
(2) Köhler, F. H.; Hofmann, P.; Prossdorf, W. *J. Am. Chem. Soc.* **1981**, *103*, 6359−6367.
(3) Curtis, C. J.; Smart, J. C.; Robbins, J. L. *Organometallics* **1985**, *4*, 1283−1286.
(4) Lauher, J. W.; Hoffmann, R. *J. Am. Chem. Soc.* **1976**, *98*, 1729−1742.
(5) Brintzinger, H. H.; Bartell, L. S. *J. Am. Chem. Soc.* **1970**, *92*, 1105−1107.
(6) Brintzinger, H. H.; Lohr, L. L.; Wong, K. L. T. *J. Am. Chem. Soc.* **1975**, *97*, 5146−5155.
(7) Petersen, J. L.; Lichtenberger, D. L.; Fenske, R. F.; Dahl, L. F. *J. Am. Chem. Soc.* **1975**, *97*, 6433−6441.
(8) Fieselmann, B. F.; Stucky, G. D. *J. Organomet. Chem.* **1977**, *137*, 43−54.
(9) Albright, T. A.; Burdett, J. K.; Whangbo, M. H. *Orbital Interactions in Chemistry*; Wiley: New York, 1985.
(10) Petersen, J. L.; Dahl, L. F. *J. Am. Chem. Soc.* **1975**, *97*, 6416−6422.
(11) Petersen, J. L.; Dahl, L. F. *J. Am. Chem. Soc.* **1975**, *97*, 6422−6433.

0002-7863/96/1518-1719$12.00/0

π-donor ability of X. By comparing the energy of this transition to that of a complex with a σ-only ligand, Cp^*_2TiH, the amount of destabilization of b_2 due to π-bonding can be quantified. A combination of optical and EPR spectra of these complexes can be used to rank ligands according to the strength of their π-interaction with the Cp^*_2Ti fragment.

Theory

For a Cp^*_2TiX complex, three d−d absorptions are expected: $1a_1 \rightarrow b_2$, $1a_1 \rightarrow b_1$, and $1a_1 \rightarrow 2a_1$ in order of increasing energy (see Figure 1). The $1a_1 \rightarrow a_2$ transition should be similar in energy to the $1a_1 \rightarrow b_1$ and $1a_1 \rightarrow 2a_1$ absorptions, but the $1a_1 \rightarrow a_2$ transition is electric dipole forbidden and should be weak or unobserved. Of the three absorptions, two should be to higher energy, $1a_1 \rightarrow 2a_1$ and $1a_1 \rightarrow b_1$, and one should be much lower in energy, $1a_1 \rightarrow b_2$. Of the two higher energy transitions, the $1a_1 \rightarrow 2a_1$ transition will have greater intensity because this orbital is σ-antibonding toward X and the $1a_1 \rightarrow 2a_1$ transition should have some charge transfer character.[12] The $1a_1 \rightarrow b_1$ transition should be less intense but somewhat similar in energy. The b_1 orbital is Ti−Cp* antibonding and Ti−X π-antibonding if the X ligand has a filled orbital of b_1 symmetry capable of acting as a π-donor (*e.g.* the nitrogen lone pair of $Cp^*_2TiN(Me)Ph$). The $1a_1 \rightarrow b_2$ transition will be much lower in energy.

The EPR spectra are closely related to the electronic spectra. As shown by McGarvey, the deviation of the g_i values from g_0 is due to coupling of excited states into the ground state as shown in eq 1 where

$$g_i = g_0 - 2\xi\sum_n \frac{\langle 0|L_i|n\rangle\langle n|L_i|0\rangle}{E_n - E_0} \qquad (1)$$

i is x, y, or z; ξ is the spin−orbit coupling constant, $E_n - E_0$ is the difference in energy of the orbitals, and the sum is over all orbitals containing d-character.[13] For bent metallocenes, Petersen and Dahl have shown that the relationship of the g values to the energies of the excited states is as shown in eq 2, where ξ is the spin−orbit coupling constant

$$g_x = g_0 - \frac{2\xi k_x^2(a\sqrt{3}+b)^2}{\Delta E_{yz}}; \quad g_y = g_0 - \frac{2\xi k_y^2(a\sqrt{3}-b)^2}{\Delta E_{xz}}; \quad g_z = g_0 - \frac{8\xi k_z^2 b^2}{\Delta E_{xy}} \qquad (2)$$

for Ti(III), 154 cm^{-1}, g_0 is 2.002 (the value of g for a free electron), ΔE_{yz}, ΔE_{xy}, and ΔE_{xz} are the energies of the excited states of d_{yz}, d_{xy}, and d_{xz} character relative to $1a_1$, that is, the a_2, b_1, and b_2 orbitals, respectively, and a and b are the coefficients of d_{z^2} and $d_{x^2-y^2}$ in the ground state, $\Psi = a|d_{z^2}\rangle + b|d_{x^2-y^2}\rangle$. The k^2 terms have been added to the original equations to account for covalency.[10,11] Since ΔE_{yz} is not measured, only the last two relationships of eq 2 will be used. The use of eq 2 implicitly assumes that only spin−orbit coupling to the unoccupied d-orbitals is important. Since the d-orbitals are involved in bonding, some low-lying orbitals will also have d-character and could potentially affect the value of g. However, since these orbitals are much further in energy from $1a_1$ and contain little d-orbital character,[1] they are not expected to change g to any great extent.

Because it is not possible to derive the values of a, k_y^2, and k_z^2 from only the last two relationships of eq 2, the assumption that $k_y^2 = k_z^2 = k^2$ is made implying that the covalency is isotropic. Since these orbitals are involved in bonding to the Cp* versus X ligands, this assumption might not be true.[14] Substituting the parameters k^2, a', and b' for k_y^2, k_z^2, a, and b gives the following equation (eq 3) which is applicable whether the covalency is anisotropic ($k_y^2 \neq k_z^2$) or isotropic ($k_y^2 = k_z^2$).

$$g_y = g_0 - \frac{2\xi k^2(a'\sqrt{3}-b')^2}{\Delta E_{xz}}; \quad g_z = g_0 - \frac{8\xi k^2 b'^2}{\Delta E_{xy}} \qquad (3)$$

$$\frac{a'}{b'} = \frac{1}{\sqrt{3}}\left[1 + \sqrt{\frac{k_y^2}{k_z^2}}\left(\frac{a\sqrt{3}}{b} - 1\right)\right]; \quad k^2 = \frac{b^2 k_z^2}{b'^2}; \quad a'^2 + b'^2 = 1$$

The parameters a', b', and k^2 no longer have a direct physical meaning, but allow the transition energies to be determined if the covalency is anisotropic. If the covalency actually is isotropic ($k_y^2 = k_z^2$), then a' and b' are the same as a and b. From the relative energies of the b_1 and b_2 orbitals, it is likely that $k_y^2 \geq k^2 \geq k_z^2$, so b will be slightly larger than b'. If g_y, ΔE_{xz}, g_z, and k^2 are known, eq 3 can be used to obtain ΔE_{xz}.

Equation 3 helps assign the EPR spectra of the Cp^*_2TiX complexes. Since ΔE_{xz} ($1a_1 \rightarrow b_2$) is much smaller than ΔE_{yz} or ΔE_{xy} and since a will be much greater than b (in $(MeCp)_2VCl_2$, $a^2/b^2 = 20$), g_y will be the g component with the smallest value. In addition, since ΔE_{xz} changes depending upon the π donor ability of X, g_y will also change greatly among the complexes. Since b is much smaller than a, g_z will have the largest value and be close to g_0. The middle component of the EPR spectra will be g_x.

Results

The syntheses of the titanium complexes were straightforward. Teuben has shown that Cp^*_2TiCl is a useful synthon for the preparation of Cp^*_2TiX complexes by chloride metathesis.[15,16] This synthetic route was used to prepare additional examples of Cp^*_2TiX where X = F, N(Me)H, OMe, or OPh, all potential π-donor ligands. The brown-purple methoxide and phenoxide and the lilac colored methylamide are soluble in hexane from which they were crystallized. The N−H stretching frequency of the methylamide is a sharp, low-intensity feature found at 3370 cm^{-1} in the solid state. The salt elimination metathesis did not yield the simplest amide, $Cp^*_2TiNH_2$, cleanly; however, this amide was prepared from Cp^*_2TiMe and ammonia in hexane from which it was crystallized. The infrared spectrum shows a single, sharp N−H absorption at 3437 cm^{-1} in the solid state.

The fluoride, Cp^*_2TiF, was synthesized in two steps. First, the difluoride, $Cp^*_2TiF_2$, was prepared by the method used by Lappert to make Cp_2TiF_2, the reaction of $Cp^*_2TiMe_2$ with $BF_3{\cdot}OEt_2$ in diethyl ether.[17] Curiously, the difluoride is almost identical in color and solubility to $Cp^*_2TiMe_2$; consequently, the reaction proceeded with little color change. Reduction of the difluoride with potassium−graphite[18] gave Cp^*_2TiF as green crystals from hexane. Recently, Cp^*_2TiF has also been prepared by the reaction of Cp^*_2TiCl with Me_3SnF.[19]

The solid-state structure of $Cp^*_2TiN(Me)H$ is shown in Figure 2, and is almost identical to that of the amide $Cp^*_2TiNH_2$.[20] Useful bonding parameters are listed in Table 1. The most interesting aspect of the crystal structure is the orientation of the methylamide ligand which adopts the least sterically favorable conformation. In $Cp^*_2TiNH_2$, the amide group adopts a similar conformation. The methylamide group lies just slightly out of the plane formed by the titanium atom and the two ligand centroids with a Cp1−Ti−N−C21 torsion angle of 13.5°. The

(12) Lever, A. B. P. *Inorganic Electronic Spectroscopy*, 2nd ed.; Elsevier: New York, 1984.

(13) McGarvey, B. R. In *Transition Metal Chemistry, a Series of Advances*; Carlin, R. L., Ed.; Marcel Dekker, Inc.: New York, 1966; Vol. 3, pp 90−201.

(14) As noted by one of the reviewers of the earlier manuscript.

(15) Luinstra, G. A.; ten Cate, L. C.; Heeres, H. J.; Pattiasina, J. W.; Meetsma, A.; Teuben, J. H. *Organometallics* **1991**, *10*, 3227−3237.

(16) Pattiasina, J. W.; Heeres, H. J.; van Bolhuis, F.; Meetsma, A.; Teuben, J. H. *Organometallics* **1987**, *6*, 1004−1010.

(17) Druce, P. M.; Kingston, B. M.; Lappert, M. F.; Spalding, T. R.; Srivastava, R. C. *J. Chem. Soc. A* **1969**, 2106−2110.

(18) Schwindt, M. A.; Lejon, T.; Hegedus, L. B. *Organometallics* **1990**, *9*, 2814−2819.

(19) Herzog, A.; Liu, F.; Roesky, H. W.; Demsar, A.; Keller, K.; Noltemeyer, M.; Pauer, F. *Organometallics* **1994**, *13*, 1251−1256.

(20) Brady, E.; Lukens, W.; Telford, J.; Mitchell, G. *Acta. Crystallogr.* **1994**, *C51*, 558−560.

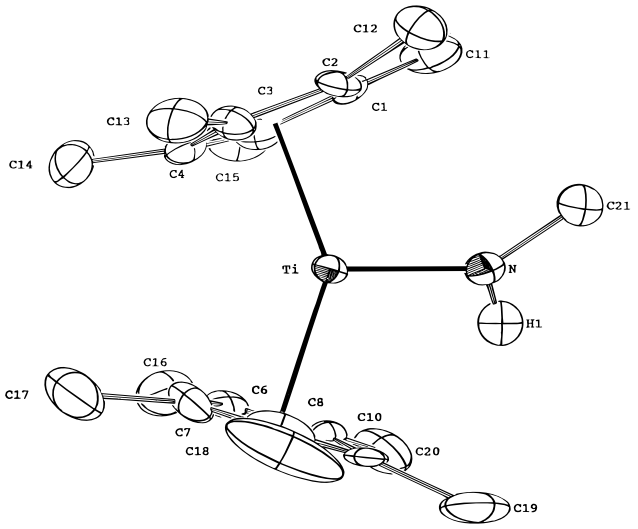

Figure 2. ORTEP drawing of $(Me_5C_5)_2TiN(Me)H$ with 50% probability thermal ellipsoids.

Table 1. Selected Distances and Angles in $Cp^*_2TiN(Me)H$

distances, Å		angles, deg	
Ti−N	1.955(5)	Cp1−Ti−Cp2	141.7
Ti−Cp1	2.084	Cp1−Ti−N−C21	13.5
Ti−Cp2	2.094	N−Ti−Cp1	110.4
Ti−⟨C_{ring}⟩	2.41(2)	N−Ti−Cp2	107.9
N−H1	0.77(7)	C21−N−H1	105 (5)
N−C21	1.446(8)	Ti−N−H1	110 (5)
		Ti−N−C21	144.9 (5)

steric interaction of the amide methyl group with the Cp* ligand bends the amide group "down" opening the Ti−N−Me angle to 145° rather than the 120° expected for an sp^2-hybridized nitrogen atom. In $Cp^*_2TiNH_2$, the Ti−N−H angle is only 126°. Stabilization of the nitrogen lone pair by interaction with the empty b_2 orbital is presumably the reason the methylamide ligand adopts this conformation. A similar explanation was given for the orientation of the methylamide ligand in the solid-state structure of $Cp^*_2Hf(H)N(Me)H$.[21]

In contrast to the orientation of the amide group in $Cp^*_2TiN(Me)H$, the crystal structure of $Cp^*_2TiN(Me)Ph$[22] shows that the *N*-methylanilide ligand is perpendicular to the Cp^*_2Ti fragment with a Cp(centroid)−Ti−N−Me torsion angle of *ca.* 90° preventing the nitrogen lone pair from acting as a π-donor to the empty b_2 orbital. In $Cp^*_2TiNH_2$ and $Cp^*_2TiN(Me)H$, the conformation of the amide group relative to Cp^*_2Ti implies maximum Ti−N π-bonding while in $Cp^*_2TiN(Me)Ph$, the conformation of the amide group implies minimal π-bonding. The Ti−N bond distances are consistent with this hypothesis. In $Cp^*_2TiNH_2$ and $Cp^*_2TiN(Me)H$, the Ti−N bond distances are 1.944(2) and 1.955(2) Å, respectively, while the Ti−N bond distances of $Cp^*_2TiN(Me)Ph$ is 2.054(2) Å. Other than the orientation of the amide ligand and the short Ti−N bond length, the crystal structure is unremarkable. The other structural features are similar to related crystallographically characterized Cp^*_2TiX compounds.[15,16,20,22]

The crystal structure analysis of Cp^*_2TiF revealed two crystallographically independent but virtually identical molecules in the asymmetric unit, one of which is shown in Figure 3. The important bond parameters for both independent molecules are listed in Table 2. The Ti−F bond lengths are short at 1.845(4) and 1.838(4) Å. However, as seen in Figure 3, the fluorine atoms have large thermal parameters making the bond lengths seem shorter. The bonds lengths corrected for the thermal motion using the root-mean-square displacements are 1.860 and 1.855 Å, respectively.[23] The corrected bond distances are 0.5 Å shorter that the Ti−Cl distance of 2.363(1) Å in Cp^*_2TiCl[16] in agreement with the size difference between chloride and fluoride.[24] Like $Cp^*_2TiN(Me)H$, the rest of the structure of Cp^*_2TiF is similar to the other known Cp^*_2TiX structures.[15,16,20,22]

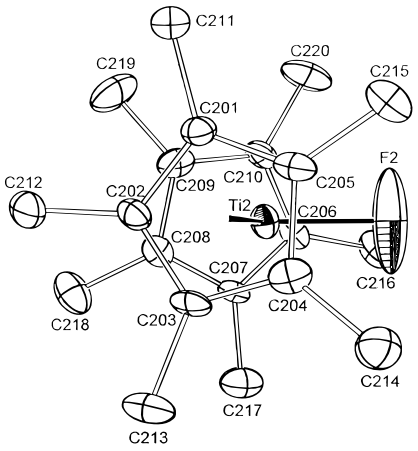

Figure 3. ORTEP drawing of $(Me_5C_5)_2TiF$ with 50% probability thermal ellipsoids.

Table 2. Selected Distances (Å) and Angles (deg) in Cp^*_2TiF

molecule 1		molecule 2	
Ti1−F1	1.845(4)	Ti2−F2	1.838(4)
Ti1−⟨C_{ring}⟩	2.38(2)	Ti2−⟨C_{ring}⟩	2.38(2)
Ti1−Cp1	2.06	Ti2−Cp3	2.05
Ti1−Cp2	2.06	Ti2−Cp4	2.05
Cp1−Ti1−Cp2	1.44.1	Cp3−Ti2−Cp4	145.6
Cp1−Ti1−F1	107.3	Cp3−Ti2−F2	106.3
Cp2−Ti1−F1	108.5	cp4−Ti2−F2	108.0

The EPR spectra of the new compounds and several known Cp^*_2TiX compounds[15,16,25] were measured as methylcyclohexane solutions at room temperature and as frozen glasses. The EPR results are listed in Table 3. For Cp^*_2TiBr and Cp^*_2TiI, the EPR parameters were obtained from the simulated spectra. Like the spectra of Cp^*_2TiBr and Cp^*_2TiI,[25] the spectra of Cp^*_2TiH and Cp^*_2TiF display ligand hyperfine coupling at low temperature. The EPR spectra and simulations for some of these complexes are shown in Figure 4. The spectra were assigned as outlined above.

The electronic spectra of several Cp^*_2TiX were measured at room temperature as 10^{-2} M solutions in methylcyclohexane. The spectrum of Cp^*_2TiOMe is shown Figure 5. In addition, the spectra of Cp^*_2TiEt and $Cp^*_2TiN(Me)Ph$ at −78 °C are shown in Figure 6 along with the least-squares fits used to obtain the peak positions. The spectra were fit using a sum of Gaussian peaks. The energies of the peaks determined in this way are listed in Table 4. In the visible region, two peaks are present for all complexes: a more intense peak at higher energy and a less intense peak at lower energy. In the near-infrared, weak transitions are observed for some of the compounds. The energy of the near-IR absorption varies from 5630 cm^{-1} for Cp^*_2TiF

(21) Hillhouse, G. L.; Bulls, A. R.; Santarsiero, B. D.; Bercaw, J. E. *Organometallics* **1988**, *7*, 1309−1312.
(22) Feldman, J.; Calabrese, J. C. *J. Chem. Soc, Chem. Commun.* **1991**, 1042−1044.
(23) Dunitz, J. *X-Ray Analysis and the Structure of Organic Molecules*; Cornell University Press: Ithaca, New York, 1979.
(24) Pauling. L. *The Nature of the Chemical Bond*; Cornell University Press: Ithaca, New York, 1960.
(25) Mach, K.; Raynor, B. *J. Chem. Soc., Dalton Trans.* **1992**, 683−688.

Table 3. EPR Data for Cp^*_2TiX Compounds (Ligand Hyperfine Coupling Constant in Parentheses in MHz)

compd	g_{ave}[a]	$\langle g \rangle$[b]	g_z[c]	g_x	g_y
Cp^*_2TiH	*d*	1.916	1.997(39)	1.981	1.780
Cp^*_2TiI	1.939	1.941	1.997	1.973(36)	1.852
$Cp^*_2TiCH_2Ph$	1.948	1.948	1.996	1.978	1.870
$Cp^*Ti(\eta^6\text{-}H_2CC_5Me_4)$	1.950	1.954	1.997	1.985	1.880
$Cp^*_2TiCH_2CMe_3$	1.951	1.952	1.998	1.984	1.881
Cp^*_2TiBr	1.953	1.953	1.996(12)	1.980(21)	1.883
$Cp^*_2Ti(n\text{-}Pr)$	1.953	1.955	1.998	1.984	1.884
Cp^*_2TiCl	1.956	1.957	1.999	1.984	1.889
Cp*2TiN(Me)Ph	1.958	1.972	1.999	1.981	1.937
$Cp^*_2TiN(Et)Ph$	1.955	1.958	1.998	1.980	1.895
Cp^*_2TiMe	1.958	1.959	1.998	1.981	1.898
$Cp^*_2TiNMe_2$	1.962	1.967	1.998	1.979	1.924
Cp^*_2TiF	1.972	1.973	1.998(37)	1.982	1.938
Cp^*_2TiEt	1.972	1.985	2.000	1.982	1.974
Cp^*_2TiOPh	1.974	1.976	1.999	1.983	1.945
Cp^*_2TiOMe	1.977	1.979	1.999	1.981	1.956
$Cp^*_2TiNH_2$	1.979	1.980	1.998	1.981	1.962
$Cp^*_2TiN(Me)H$	1.980	1.981	1.998	1.980	1.965

[a] The averaged *g*-values in solution at room temperature. [b] $\langle g \rangle = {}^1/_3(g_x + g_y + g_z)$. [c] The anisotropic *g*-values from frozen solutions. [d] Unobserved.

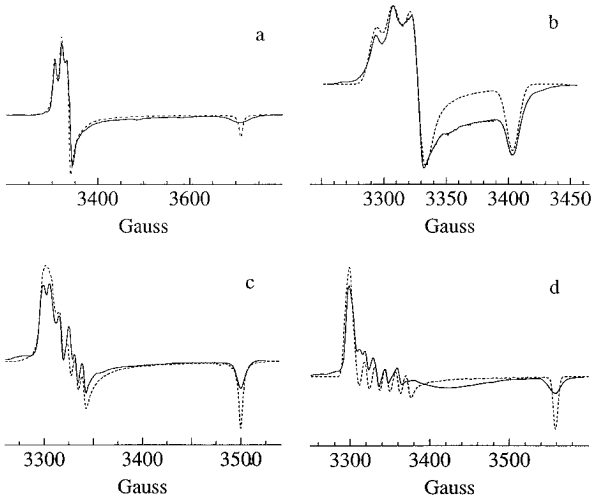

Figure 4. EPR spectra (solid lines) and simulations (dotted lines) of $(Me_5C_5)_2TiH$ (a), $(Me_5C_5)_2TiF$ (b), $(Me_5C_5)_2TiBr$ (c), and $(Me_5C_5)_2TiI$ (d) in a methylcyclohexane glass at *ca.* 70 K.

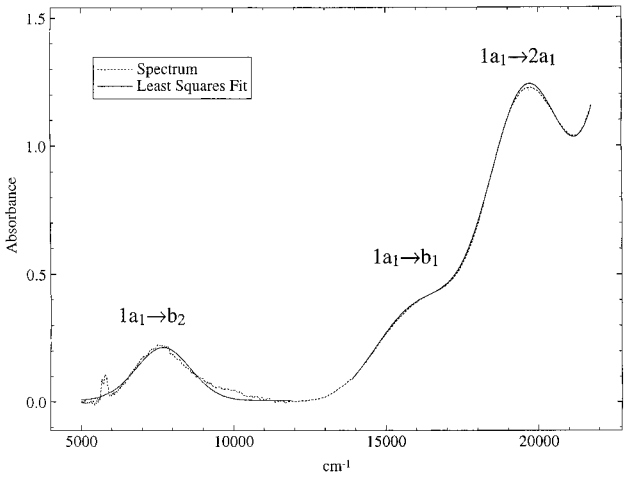

Figure 5. Electronic spectrum of Cp^*_2TiOMe in methylcyclohexane at 298 K.

to 8220 cm^{-1} for $Cp^*_2TiN(Me)H$. No near-infrared absorption was observed for many of the compounds presumably because it was too low in energy. The spectra were assigned as outlined above.

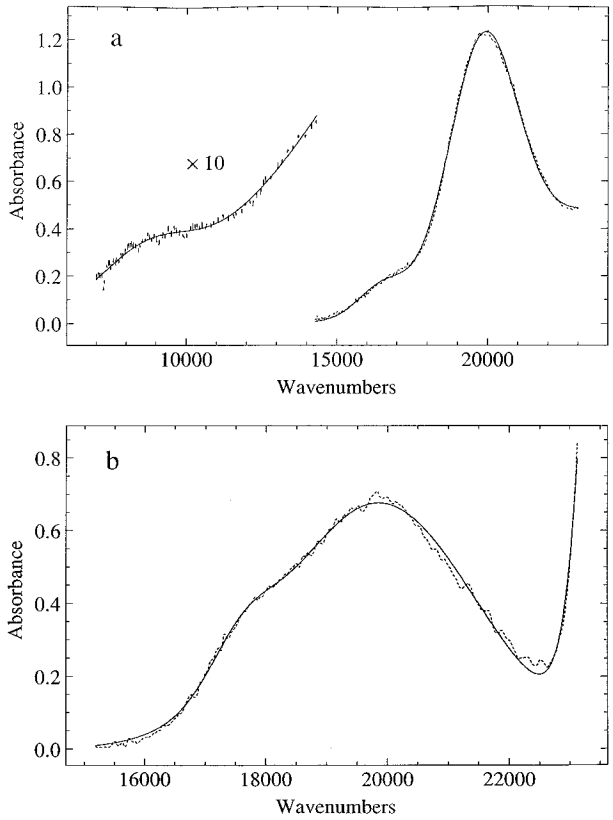

Figure 6. Electronic spectra (dotted lines) and least-squares fits (solid lines) of Cp^*_2TiEt (a) and $Cp^*_2TiN(Me)Ph$ (b) at 77 K.

Table 4. Electronic Transitions of Cp^*_2TiX Complexes in cm^{-1} (The Extinction Coefficient, L cm^{-1} mol^{-1}, Is in Parentheses)

	T (in K)	$1a_1 \rightarrow 2a_1$	$1a_1 \rightarrow b_2$ (ΔE_{xz})	$1a_1 \rightarrow b_1$ (ΔE_{xy})
Cp^*_2TiH	295	20976(131)		18272(69)
Cp^*_2TiI	295	16065(135)		14610(51)
$Cp^*_2TiCH_2Ph$	295	20203(173)		16017(42)
$Cp^*Ti(\eta^6\text{-}Me_4C_5CH_2)$	295	23000(180)		17816(180)
$Cp^*_2TiCH_2CMe_3$	295	20340(182)		15190(29)
$Cp^*_2Ti(n\text{-}Pr)$	295	21702(189)		17342(63)
Cp^*_2TiBr	295	17260(131)		15023(40)
Cp^*_2TiCl	295	18118(110)		15426(59)
$Cp^*_2TiN(Me)Ph$	295	19465(247)		15893(121)
$Cp^*_2TiN(Me)Ph$	77	19850		17595
Cp^*_2TiMe	295	21781(170)		16665(50)
Cp^*_2TiEt	295	20826(122)		15895(21)
Cp^*_2TiEt	77	19828	8643	16550
Cp^*_2TiF	295	23231(167)	57722(23)	17124(29)
Cp^*_2TiOPh	295	19596(134)	6544(29)	15980(51)
Cp^*_2TiOMe	295	19607(128)	7800(21)	16155(47)
$Cp^*_2TiNH_2$	295	20369(90)	7942(6)	15422(34)
$Cp^*_2TiN(Me)H$	295	19593(114)	8180(8)	15159(40)

Discussion

As noted previously, the unpaired electron occupies the $1a_1$ orbital which is largely d_{z^2} with some $d_{x^2-y^2}$ character. This orbital is nonbonding and interacts only weakly with the X ligand in Cp^*_2TiX and is, therefore, not expected to be sensitive to the σ-donor ability of X.[4] The LUMO, b_2, is mainly d_{xz} and is close to $1a_1$ in energy in the absence of π-effects. When X is a π-donor, b_2 acts as a π-acceptor and is destabilized as the extent of ligand π-donation increases. By comparing the energy of the $1a_1 \rightarrow b_2$ transition for a series of complexes to the energy of this transition of a complex with a σ-only ligand, Cp^*_2TiH, the relative strength of the π-interaction in these complexes can be determined. Since b_2 is π-antibonding, the actual strength of the π-interactions is somewhat less than the energy deter-

Table 5. Calculated Values of a', b', and k^2 from the Electronic and EPR Spectra

	b'	a'	k^2
Cp^*_2TiF	0.29	0.96	0.64
Cp^*_2TiOPh	0.25	0.97	0.60
Cp^*_2TiOMe	0.26	0.97	0.58
$Cp^*_2TiNH_2$	0.30	0.95	0.56
$Cp^*_2TiN(Me)H$	0.30	0.95	0.54

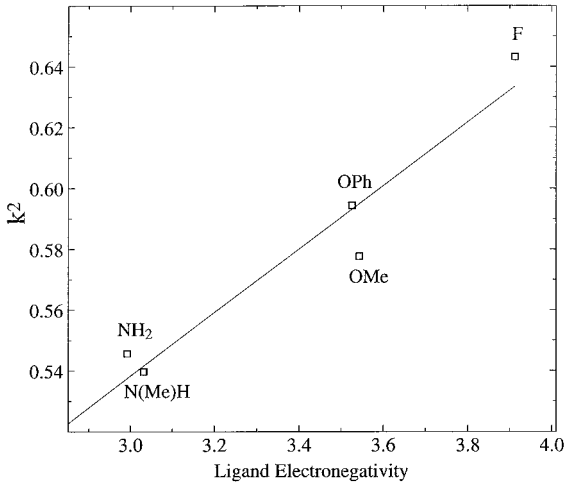

Figure 7. Observed covalency versus ligand electronegativity for some Cp^*_2TiX complexes. X is given next to the corresponding data point.

mined in this way. Thus, this method overemphasizes the π-bonding capability of X.

In the compounds for which g_y, g_z, ΔE_{xz}, and ΔE_{xy} are observed, the values of a', b', and k^2 can be calculated directly. The results are given in Table 5. The values of a' and b' vary only slightly among these complexes, and the values of a'^2/b'^2 are slightly smaller than those seen by Petersen and Dahl for Cp_2VX_2 complexes,[10,11] but are similar to those calculated for Cp_2TiS_5.[7] The fact that a' and b' have the same sign shows that $1a_1$ resides mainly in the *yz* plane (the d_{z^2} orbital is compressed along the *x* axis, see the d_{z^2} orbital in Figure 1). In contrast, Petersen and Dahl found that in the Cp_2VX_2 complexes, *a* and *b* had opposite signs, so that $1a_1$ is mainly in the *xz* plane.[10,11] However, for the related Cp_2VCO, the ratio a^2/b^2 is about the same as in Cp_2VX_2, but the signs of *a* and *b* are the same as they are for Cp^*_2TiX complexes.[26] This apparent contradiction was explained by noting that in Cp_2VCO, as in the trivalent decamethyltitanocenes, the change in sign of *b* reflects a decrease in electron density along the *x* axis which minimizes a destabilizing interaction with the σ-bonding orbital of the ligand.

Unlike the values of a' and b', the value of k^2 changes with the ligand. The greater the ligand electronegativity,[27] the higher the value of k^2. As seen in Figure 7, this relationship is roughly linear. The less electronegative ligands have a more covalent interaction with the titanium center, decreasing k^2 for the unpaired electron.

The transition energy ΔE_{xz} was calculated using the *g* values from the EPR spectra, the observed value of ΔE_{xy}, and k^2 values estimated using the linear relationship shown in Figure 7. The results, along with the values of a' and b', are listed in Table 6. The values of ΔE_{xz} calculated from the EPR spectra agree fairly well with those obtained from the near-infrared spectra.

The amount of destabilization of b_2 caused by the π-donor ligand is determined by comparing ΔE_{xz} to the value of ΔE_{xz} in Cp^*_2TiH. A potential problem exists, however, in that Lauher and Hoffmann have predicted that the hydride ligand does not lie on the *x*-axis.[4] This distortion increases the value of ΔE_{xz} for Cp^*_2TiH from a true σ-only value since the σ-orbital of the hydride ligand will interact with the b_2-orbital. However, more recent calculations suggest that the hydride ligand does lie along the *x*-axis.[28] It should be noted that the CH_2CMe_3 ligand of $Cp^*_2TiCH_2CMe_3$ does not lie on the *x*-axis,[15] and the destabilization of the b_2 orbital in this complex is 550 cm^{-1} greater than the destabilization of b_2 in $Cp^*_2TiCH_2C_6H_5$. Presumably, the less sterically demanding benzyl ligand does lie on the *x*-axis. The relatively high value of b' for this complex is disturbing since this observation implies that the bonding in Cp*TiH is different from that in the other metallocenes.

Table 6. Calculated Values for Cp^*_2TiX Complexes

	b'	a'	ΔE_{xz}(calc)	ΔE_{xz}(obs)	ΔE_{xz} relative to Cp^*_2TiH
Cp^*_2TiH	0.57	0.82	447		0
Cp^*_2TiI	0.36	0.93	1537		1090
$Cp^*_2TiCH_2C_6H_5$	0.40	0.92	1601		1154
$Cp^*Ti(\eta^6\text{-}Me_4C_5CH_2)$	0.39	0.92	1794		1348
$Cp^*_2TiCH_2CMe_3$	0.32	0.95	2157		1710
$Cp^*_2Ti(n\text{-}Pr)$	0.34	0.94	2096		1649
Cp^*_2TiBr	0.38	0.92	1923		1476
Cp^*_2TiCl	0.27	0.96	2852		2405
$Cp^*_2TiN(Me)Ph$	0.28	0.96	4870		4423
Cp^*_2TiMe	0.33	0.94	2410		1963
Cp^*_2TiF	0.29	0.96	5622	5738	5175
Cp^*_2TiOPh	0.25	0.97	6445	6563	5998
Cp^*_2TiOMe	0.26	0.97	7995	7700	7549
$Cp^*_2TiNH_2$	0.30	0.95	7479	7633	7032
$Cp^*_2TiN(Me)H$	0.30	0.95	8217	8180	7770
Cp^*_2TiEt[a]	0.33	0.94	8695	8460	8248

[a] Not used in determining the k^2 relationship.

A geometric distortion, *e.g.* bending of the hydride ligand, could be responsible for the difference in bonding suggested by the high value of b' for Cp^*_2TiH. Its structure shows that the hydride ligand does indeed lie on the *x*-axis of the molecule. However, the metallocene angle ($\angle$Cp*−Ti−Cp*), 152°, is much greater than that in other decamethyltitanocenes.[29] The larger metallocene angle in Cp^*_2TiH is the geometric distortion responsible for the higher value of b' in this complex. As the metallocene angle increases, the d_{z^2} and $d_{x^2-y^2}$ orbitals become closer in energy and will interact more strongly, giving $1a_1$ more $d_{x^2-y^2}$ character relative to the other complexes.[4] The larger metallocene angle in Cp^*_2TiH makes ΔE_{xz} somewhat smaller than it would be if the metallocene angle were the same as in a normal Cp^*_2TiX complex. Consequently, using ΔE_{xz} of Cp^*_2TiH as the anchor for the π-bonding ability of X will, again, tend to overestimate the π-bond strength.

Among the halides, the trend in π-bond strengths is F > Cl > Br > I. This trend has been observed previously in other analyses of bonding in bent metallocenes and has been attributed to strong overlap between the p-orbitals of the halide and the d-orbitals of the bent metallocene fragment.[30,31] Furthermore, fluoride is a fairly good π-donor, only slightly weaker than phenoxide. The trend in π-bond strengths agrees with the trend seen in octahedral Cr(III) complexes.[12]

A potential problem exists in the analysis of the halides since the observed spin−orbit coupling could increase due to ligand

(26) Razuvaev, G. A.; Abakumov, G. A.; Cherkasov, V. K. *Russ. Chem. Rev.* **1985**, *54*, 1235−1259.
(27) Inamoto, N.; Masuda, S. *Chem. Lett.* **1982**, 1003−1006.
(28) Bierwagen, E. P.; Bercaw, J. E.; Goddard, W. A., III *J. Am. Chem. Soc.* **1994**, *116*, 1481−1489.
(29) Lukens, W. W.; Matsunaga, P. T.; Andersen, R. A. To be resubmitted.
(30) Hunter, J. A.; Lindsell, W. E.; McCullough, K. J.; Parr, R. A.; Scholes, M. L. *J. Chem. Soc., Dalton Trans.* **1990**, 2145−2153.
(31) Asaro, M. A.; Cooper, S. R.; Cooper, N. J. *J. Am. Chem. Soc.* **1986**, *108*, 5187−5193.

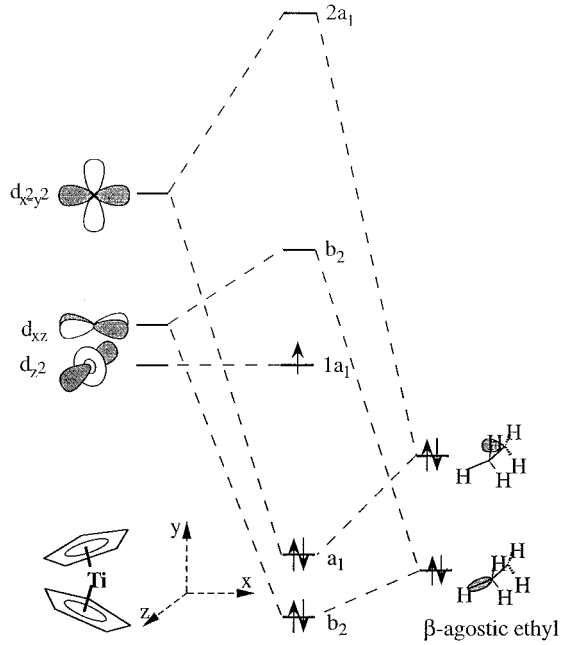

Figure 8. Destabilization of "b_2" by a β-agostic ethyl ligand. Note that the actual symmetry of the complex is C_s or C_1; however, the symmetry labels for C_{2v} are given for consistency.

character in the metallocene d-orbitals. This effect would decrease g_y by increasing ξ rather than by decreasing b_2 making the heavier halides seem like poorer π-donors than they actually are. For Cp^*_2TiI with $\xi_I = 5069$ cm^{-1},[32] this effect would be greatest, but since $3g_{ave} - g_y$ (that is, $g_x + g_z$) is approximately the same for all of these compounds, ξ does not differ greatly from that of the other complexes. In addition, based upon the small values observed for the ligand hyperfine coupling, only a small amount of ligand character is present in the $1a_1$ orbital.[33] This observation is in agreement with PES studies on Cp_2VX in which the amount of ligand character in the b_2 orbitals was found to be tiny.[1]

A more interesting observation is the high value of g_y for Cp^*_2TiEt. The magnitude of g_y implies that the ethyl ligand is a stronger π-donor than N(Me)H. The ethyl group in Cp^*_2TiEt is thought to be β-agostic based upon the observation of low-frequency C−H stretching absorption in its infrared spectrum.[15] As shown in Figure 8, a β-agostic interaction will raise the energy of b_2 in much the same way as a π-interaction. In addition to the high value of g_y, at 77 K, the $1a_1 \rightarrow b_2$ transition can be observed directly at 8640 cm^{-1}. While this energy would seem to indicate that the electronic contribution to the agostic interaction is about 8000 cm^{-1}, this is not true. If the σ-bond of the ethyl group in Cp^*_2TiEt moves off of the x-axis, b_2 will be destabilized by the σ-bond in addition to the agostic interaction, and the electronic contribution to the agostic interaction will be considerably less than 8000 cm^{-1}.

Curiously, the g_{ave} value determined from the room temperature EPR spectrum of Cp^*_2TiEt is quite different from $\langle g \rangle$, the average of the g components recorded in the frozen glass spectrum. This observation, along with the inability to observe the $1a_1 \rightarrow b_2$ transition at room temperature, led us to postulate that an equilibrium between agostic and anagostic forms of Cp^*_2TiEt is present, Figure 9.

In addition to Cp^*_2TiEt, g_{ave} and $\langle g \rangle$ are quite different in $Cp^*_2TiN(Me)Ph$. The N(Me)Ph ligand also seems to be agostic,

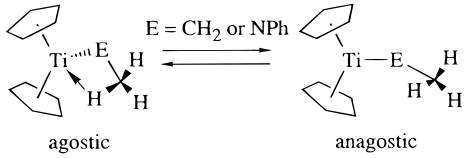

Figure 9. An equilibrium between agostic and anagostic conformers.

most likely by a β-agostic *N*-methyl group rather than a γ-agostic phenyl group since $Cp^*_2TiCH_2Ph$ shows no evidence of an agostic interaction. The presence of a β-*N*-methyl agostic interaction is supported by weak infrared absorptions at 2570 and 2620 cm^{-1} and by the published crystal structure.[22] In $Cp^*_2TiN(Me)Ph$, the N(Me)Ph ligand is planar and lies in the plane between the Cp* ligands. The Ti−N−C_{Me} angle is 110.8(2)° while the Ti−N−C_{ipso} angle is 131.6(1)°; this geometry is consistent with a β-agostic interaction. On the other hand, in the *n*-butyl isocyanide adduct, the Ti−N−C_{Me} angle is 121.2(4)° and the Ti−N−C_{ipso} angle is 125.6(4)°.[22] The geometry of the base adduct is not consistent with a β-agostic interaction. The lack of an agostic interaction is expected since the base adduct has no low-lying, empty orbitals available to form an agostic interaction.

For the equilibrium shown in Figure 9, K = [anagostic]/[agostic] = $\exp(-\Delta H°/RT + \Delta S°/R)$ where $\Delta H°$ and $\Delta S°$ are the enthalpy and entropy of the anagostic conformation relative to the agostic conformation, respectively. Based on the assumption that the observed g_{ave} value represents the weighted average of the g_{ave} values of the agostic and anagostic forms, then the formula for the observed g_{ave} value is given in eq 4 where $g_{agostic}$ is the g_{ave} value for the agostic conformation, $g_{anagostic}$ is the g_{ave} value for the anagostic conformation, and $\Delta H°$ and $\Delta S°$ are as defined earlier.

$$g_{obs} = \frac{1}{K+1}(g_{agostic} + Kg_{anagostic})$$

$$K = e^{-(\Delta H° - T\Delta S°)/RT} \qquad (4)$$

Fitting the g_{ave} values from the variable-temperature EPR spectra of these complexes with eq 4, using the average of the g components observed in the frozen glass spectra for $g_{agostic}$, will give the values of the unknowns, $\Delta H°$, $\Delta S°$, and $g_{anagostic}$. Plots of g_{iso} versus T for Cp^*_2TiEt and $Cp^*_2N(Me)Ph$ are shown in Figure 10. For Cp^*_2TiEt, the variable-temperature EPR data from −98 to 68 °C yield $\Delta H° = 1.93(3)$ kcal/mol, $\Delta S° = 6.3(2)$ eu, and $g_{anagostic} = 1.9570(7)$. For $Cp^*_2TiN(Me)Ph$ from −58° to 105 °C, the values are $\Delta H° = 1.5(1)$ kcal/mol, $\Delta S° = 7.9(5)$ eu, and $g_{anagostic} = 1.9545(3)$. The data are for three separate runs for each complex and assume an error of 1×10^{-4} in g_{ave} (based upon $\sigma(g_{ave})$ for spectra acquired at the same temperature).

The entropy difference between the agostic and anagostic molecules is the same in both cases. The entropy difference can be estimated by $R \ln(\sigma)$ where σ is the product of the symmetry numbers of the anagostic molecule versus the agostic molecule.[34] Assuming all of the ligands are freely rotating, then the anagostic molecule has C_{2v} symmetry ($\sigma = 2$) while the agostic molecule has C_s symmetry ($\sigma = 1$). Additionally, in the agostic molecule, a 3-fold methyl rotation and a 2-fold Ti−Et or Ti−N(Me)Ph rotation are being stopped. The symmetry difference σ is $3 \times 2 \times 2$ and $R \ln(\sigma)$ is 4.9 in rough agreement with the observed value of $\Delta S°$.

(32) Moore, C. E. Atomic Energy Levels As Derived From the Analyses of Optical Spectra. National Bureau of Standards, 1958.

(33) Weltner, W., Jr. *Magnetic Atoms and Molecules*; Dover Publications, Inc.: New York, 1983.

(34) Lowry, T. H.; Richardson, K. S. *Mechanism and Theory in Organic Chemistry*, 3rd.; Harper & Row: New York, 1987.

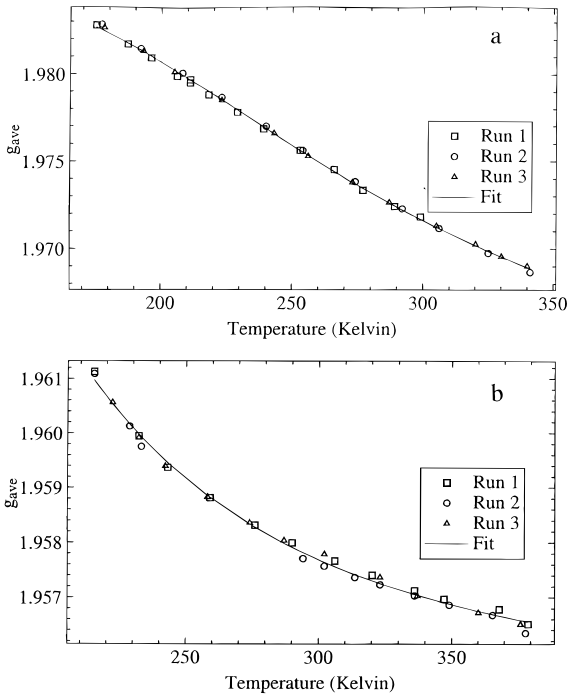

Figure 10. Observed g_{ave} versus temperature for Cp^*_2TiEt (a) and $Cp^*_2TiN(Me)Ph$ (b). The different symbols are for independent data runs, and the line is a least-squares fit to eq 4.

The $g_{anagostic}$ values for Cp^*_2TiEt and $Cp^*_2TiN(Me)Ph$ are very similar to the g_{ave} values of Cp^*_2TiMe (1.958) and $Cp^*_2TiN(Et)Ph$ (1.955) as expected. The $g_{anagostic}$ values can be used to estimate the g_y value for the anagostic form of the molecules by assuming that g_z and g_x are the same in both conformations. For Cp^*_2TiEt and $Cp^*_2TiN(Me)Ph$, the g_y values for the anagostic conformation are 1.890 and 1.884, respectively. If the optical spectra are known for the agostic and anagostic conformers, the change in the $1a_1 \rightarrow b_2$ energy between them can be estimated. This energy gives the electronic contribution to the agostic bond.

From the values of $\Delta H°$ and $\Delta S°$, at 20 °C the constants for the equilibrium in Figure 9 for Cp^*_2TiEt and $Cp^*_2TiN(Me)Ph$ are 0.87 and 4.1, respectively. The equilibrium constants help to explain why no $1a_1 \rightarrow b_2$ transition is observed for Cp^*_2TiEt or $Cp^*_2TIN(Me)Ph$ at room temperature. For $Cp^*_2TiN(Me)$-Ph, most of the molecules have no agostic interaction and for Cp^*_2TiEt approximately 45% have no agostic interaction. While the transferability of the solution data to a frozen glass is uncertain, at 77 K, the equilibrium constants for Cp^*_2TiEt and $Cp^*_2TiN(Me)Ph$ are 8×10^{-5} and 3×10^{-3}, respectively. Spectra acquired at that temperature are expected to be due only to the agostic species. The spectra of Cp^*_2TiEt and Cp^*_2TiN-(Me)Ph in toluene-d_8 at 77 K are shown in Figure 6. Unfortunately, the $1a_1 \rightarrow b_2$ transition for $Cp^*_2TiN(Me)Ph$ was not observed due to the presence of C−H or C−D stretching overtones from the solvent.

As noted earlier, the combined electronic and EPR data can be used to estimate the electronic contribution to the agostic bond. For Cp^*_2TiEt, b_2 is destabilized by 18 kcal/mol in the agostic conformation, but some of the destabilization is likely the result of the σ-bond of the ethyl ligand moving off of the *x*-axis. This is shown by the observation that at 77 K, the $1a_1 \rightarrow 2a_1$ transition is 1000 cm^{-1} lower in energy than at room temperature and 2000 cm^{-1} lower than in Cp^*_2TiMe indicating that the ethyl group is interacting more weakly with the $2a_1$ as it moves off the *x*-axis. In $Cp^*_2TiN(Me)Ph$, in which N(Me)-Ph lies on the *x*-axis, b_2 is destabilized by 6 kcal/mol in the agostic conformation.

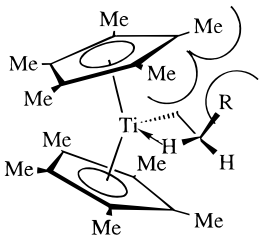

Figure 11. Steric congestion in a β-agostic alkyl complex of Cp^*_2Ti.

In both complexes, the enthalpy difference, $\Delta H°$, is quite a bit smaller than the destabilization of the b_2 orbitals. The destabilization of b_2 reflects only the electronic contribution to the agostic bond. The electronic contribution is greater than the net interaction since it does not reflect destabilization of the agostic conformation due to steric crowding or strain caused by bending the ligand. The net enthalpy, $\Delta H°$, of the agostic bond is also much smaller than in agostic bonds in other complexes. For example, in $(Cy_3P)_2(CO)_3W$ (Cy = cyclohexyl) one of the PCy_3 ligands has a γ-agostic interaction with the tungsten center. The strength of the agostic interaction is estimated to be 16 kcal/mol.[35] Additionally, theoretical calculations on the molecule $Ti(Et)Cl_3(dmpe)$ (dmpe = 1,2-bis-(dimethylphosphino)ethane) show that the agostic form is 12.4 kcal/mol lower in energy than the anagostic conformation.[36,37] In comparing this energy to that of the Cp^*_2TiX complexes, it is important to note that the strength of the agostic interaction in a titanium(III) complex is expected to be weaker than that for an analogous titanium(IV) complex since titanium(IV) complex is more electrophilic or Lewis acidic and is expected to form a stronger agostic bond. In addition, the Cp^*_2Ti environment is more sterically demanding than either of these two examples (the Cy_3P ligand is large, but its bulk is well away from the tungsten center).

The fact that the agostic interaction in Cp^*_2TiEt is so weak explains why the other alkyl complexes of Cp^*_2Ti do not form β-agostic bonds. As shown in Figure 11, the substituent on the β-carbon atom will have an unfavorable steric interaction with the Cp* ligand. If the steric repulsions in the β-agostic conformations of other alkyl groups are more than 2 kcal/mol greater than in Cp^*_2TiEt, the agostic conformation will be unfavorable relative to the anagostic conformation. The lack of α- or γ-agostic interactions can be rationalized in a similar manner.

In conclusion, electronic and EPR spectroscopy can be used to rank the X ligands of Cp^*_2TiX in terms of π-donating ability. The π-donor series is similar to that seen in other systems. No evidence is seen for α- or γ-agostic interactions in the trivalent decamethyltitanocene alkyl complexes, but β-agostic interactions can be observed for Cp^*_2TiEt and $Cp^*_2TiN(Me)Ph$. The equilibrium between the agostic and anagostic conformations of these molecules can be examined using variable-temperature EPR spectroscopy, and the equilibrium constant is found to be 0.9 and 4 at room temperature for Cp^*_2TiEt and $Cp^*_2TiN(Me)$-Ph, respectively, and *ca.* 10^{-4} at 77 K.

(35) Gonzales, A. A.; Zhang, K.; Nolan, S. P.; Lopez de la Vega, R. L.; Murkerjee, S. L.; Hoff, C. D.; Kubas, G. J. *Organometallics* **1988**, *12*, 2429−2435.

(36) Dawoodi, Z.; Green, M. L. H.; Mtetwa, V. S. B.; Prout, K. *J. Chem. Soc., Chem. Commun.* **1982**, *12*, 802−803.

(37) Munakata, H.; Ebisawa, Y.; Takashima, Y.; Wrinn, M. C.; Sheiner, A. C.; Newsam, J. M. *Catal. Today* **1995**, *23*, 403−408.

Experimental Section

All reactions and manipulations were carried out in an inert atmosphere using standard Schlenk and drybox techniques. Ammonia and methylamine were dried over sodium at −78 °C and distilled immediately prior to use. The lithium salts of the amides were prepared by the addition of the amine to a solution of *n*-butyllithium in hexane. The lithium salts of the alkoxides were prepared by treating lithium metal with the alcohol in hexane. Cp^*_2TiBr, Cp^*_2TiI, Cp^*_2TiCl;[16] $Cp^*_2TiCH_2C_6H_5$, $Cp^*_2TiCH_2CMe_3$, $Cp^*_2Ti(n\text{-}Pr)$, Cp^*_2TiEt, Cp^*_2TiMe, Cp^*_2TiH;[15] $Cp^*_2TiN(Me)(Ph)$;[22] $Cp^*_2TiMe_2$;[38] and KC_8[18] were prepared by literature methods. Infrared spectra were recorded on a Nicolet 5DX FTIR spectrometer or a Perkin-Elmer 283 spectrometer as Nujol mulls between CsI or KBr plates. ^1H NMR spectra were measured on a JEOL FX90Q FT NMR spectrometer operating at 89.56 MHz or on a home-built FT NMR spectrometer (Cryomagnet Systems 5.9 T magnet interfaced to a Nicolet 1180 computer) operating at 250.80 MHz at the Berkeley Department of Chemistry NMR facility. Chemical shifts were referenced to tetramethylsilane ($\delta = 0$) with positive values at lower field. Melting points were measured on a Thomas-Hoover melting point apparatus in sealed capillaries and are uncorrected. EPR spectra were measured as solutions or frozen glasses in either methylcyclohexane or 2-methyltetrahydrofuran using a Varian E-12 spectrometer. For the frozen glass spectra, an Oxford Instruments ESR-10 liquid helium cryostat was used. For the variable-temperature studies, a Wilmad Version 1 variable-temperature apparatus was used; the temperature was determined using a thermocouple referenced to a 0 °C ice bath. The microwave frequency was measure using an EIP-548 microwave frequency counter and the magnetic field was measure using a Varian E-500 NMR gaussmeter. Spectra were digitized using UNPLOTIT. EPR simulations were done using the program ABVG.[39] Optical spectra were recorded as 10^{-3} to 10^{-2} M solutions in methylcyclohexane using matched quartz cells and a Cary 17 spectrophotometer controlled by a PC. For the low-temperature spectra a quartz dewar of liquid nitrogen was used, and the samples were contained in an EPR tube surrounded by a copper mask with a 2 mm wide by 7 mm high window. Spectra were fit as sums of Gaussian curves using the program Horizon.[40] Electron impact mass spectra were recorded by the mass spectroscopy laboratory at the University of California, Berkeley. Elemental analyses were performed by the analytical laboratories at the University of California, Berkeley.

$Cp^*_2TiNH_2$. Approximately 300 mL of gaseous NH_3 at room temperature (*ca*. 13 mmol) was vacuum transferred to a solution of Cp^*_2TiMe (1.20 g, 3.60 mmol) in hexane at −78 °C. The solution was allowed to warm to room temperature and the evolved gasses were periodically vented. After gas evolution had ceased, the solution was filtered and the volume of the filtrate was reduced to *ca*. 5 mL. Cooling at −80 °C gave dark crystals (0.70 g, 58%). It was necessary to dry the ammonia over sodium for at least 1 h at −78 °C to obtain spectroscopically and analytically pure material. Mp = 193−196 °C. IR: 3437 (m), 2721 (m), 1535 (s), 1491 (s), 1023 (s), 802 (w), 634 (s), 626 (m), 616 (s), 598 (s), 486 (s), 431 (s), 395 (m) cm^{-1}. MS $(M)^+$ *m/z* (found) 352 (100), 353 (30). Anal. Calcd for $C_{20}H_{32}NTi$: C, 71.8; H, 9.65; N, 4.20. Found: C, 71.7; H, 9.74; N, 4.14.

$Cp^*_2TiN(Me)H$. A mixture of Cp^*_2TiCl[16] (0.71 g, 2.0 mmol) and LiN(Me)H (0.09 g, 2.4 mmol) was suspended in 30 mL of diethyl ether. After the mixture was stirred for 12 h, the solvent was removed under reduced pressure, and the solid was suspended in 50 mL of hexane forming a lilac-colored solution. The solution was filtered, and the volume of the filtrate was reduced to *ca*. 5 mL. Cooling to −20 °C gave green crystals (0.32 g, 46%). Mp = 202−205 °C. IR 3360 (w), 2765 (m), 2725 (w), 1405 (m), 1160 (w), 1083 (s), 1037 (m), 1010 (m), 790 (w), 711 (w), 617 (w), 535 (m), 494 (s), 419 (s), 378 (m) cm^{-1}. MS $(M)^+$ *m/z* (calc, found) 347 (12, 44), 348 (100, 100), 349 (31, 32), 350 (12, 11). Anal. Calcd for $C_{21}H_{34}NTi$: C, 72.4; H, 9.84; N, 4.02. Found: C, 73.0; H, 9.89; N, 4.04.

$Cp^*_2TiF_2$. $Cp^*_2TiMe_2$[38] (1.15 g, 3.30 mmol) was dissolved in 70 mL of diethyl ether, and $BF_3{\cdot}OEt_2$ (0.96 g, 6.8 mmol) was added slowly using a syringe. The yellow solution became orange. After the mixture was stirred for 12 h, the solvent was removed under reduced pressure and the residue was heated at 90 °C under dynamic vacuum for 4 h to remove $MeBF_2$. The yellow solid residue was dissolved in 100 mL of hexane and the solution was filtered. The volume of the filtrate was reduced to *ca*. 20 mL. Cooling to −80 °C gave orange needles (1.1 g, 93%). Mp = 207−208 °C. ^1H NMR δ 1.82 (s). IR 2720 (w), 1165 (w), 1065 (w), 1020 (m), 810 (w), 725 (w), 635 (w), 610 (m), 580 (s), 565 (s), 545 (m), 440 (s), 390 (m) cm^{-1}. MS $(M)^+$ *m/z* (calc, found) 354 (10, 11), 355 (12, 12), 356 (100, 100), 357 (30, 29), 358 (11, 11), 359 (2, 2). Anal. Calcd for $C_{20}H_{30}TiF_2$: C, 67.4; H, 8.48. Found: C, 67.4; H, 8.59.

Cp^*_2TiF. A slurry a KC_8 (0.21 g, 2.0 mmol) in 20 mL of tetrahydrofuran was added by cannula to a solution of $Cp^*_2TiF_2$ (0.67 g, 1.9 mmol) dissolved in 10 mL of tetrahydrofuran. The solution immediately turned dark green. After the mixture was stirred for 3 h, the solvent was removed under reduced pressure. The solid residue was suspended in 100 mL of hexane. The dark green suspension was filtered, and the volume of the filtrate was reduced to *ca*. 10 mL. Cooling to −20 °C gave dark green crystals (0.40 g, 63%). Mp = 201−203 °C. IR 2720 (w), 1165 (w), 1065 (w), 1025 (m), 805 (w), 725 (w), 635 (w), 610 (w), 570 (s), 450 (s), 415 (w), 395 (w) cm^{-1}. MS $(M)^+$ *m/z* (calc, found) 335 (11, 16), 336 (12, 18), 337 (100, 100), 338 (30, 31), 339 (11, 12). Anal. Calcd for $C_{20}H_{30}TiF$: C, 71.1; H, 8.96. Found: C, 70.9; H, 8.94.

$Cp^*_2TiOCH_3$. A mixture of Cp^*_2TiCl[16] (0.50 g, 1.4 mmol) and $LiOCH_3$ (0.06 g, 1.6 mmol) was suspended in 40 mL of tetrahydrofuran. The solution was warmed to 70 °C for 3 h during which time the solution turned red-orange. The suspension was allowed to cool to room temperature. After the mixture was stirred for 12 h, the solvent was removed under reduced pressure, and the solid residue was suspended in 50 mL of hexane. The red-purple suspension was filtered, and the volume of the filtrate was reduced to *ca*. 1 mL. Cooling to −20 °C produced brown plates (0.33 g, 67%). Mp = 135−150 °C. IR 2790 (s), 2720 (w), 1270 (w), 1150 (s), 1075 (m), 1025 (m), 800 (w), 760 (m), 725 (w), 660 (w), 620 (w), 550 (m), 500 (m), 420 (m) cm^{-1}. MS $(M)^+$ *m/z* (calc, found) 347 (11, 4), 348 (12, 5), 349 (100, 100), 350 (31, 12), 351 (12, 5). Anal. Calcd for $C_{21}H_{33}OTi$: C, 72.2; H, 9.52. Found: C, 71.7; H, 9.65.

$Cp^*_2TiOC_6H_5$. A mixture of Cp^*_2TiCl[16] (0.50 g, 1.4 mmol) and $LiOC_6H_5$ (0.16 g, 1.6 mmol) was dissolved in 30 mL of tetrahydrofuran. The solution immediately became purple-red. After the mixture was stirred for 10 h, the solvent was removed under reduced pressure, and the residue was suspended in 50 mL of hexane. The purple suspension was filtered, and the volume of the filtrate was reduced to *ca*. 10 mL. Cooling to −20 °C gave big purple-brown crystals (0.48 g, 83%). Mp = 202−207 °C. IR: 2720 (w), 2610 (w), 1615 (w), 1585 (s), 1565 (m), 1485 (s), 1310 (s), 1160 (s), 1065 (w), 1020 (w), 995 (m), 880 (s), 750 (s), 695 (m), 630 (w), 620 (m), 605 (w), 520 (w), 430 (m), 405 (w), 360 (m) cm^{-1}. MS $(M)^+$ *m/z* (calc, found) 409 (10, 20), 410 (13, 22), 411 (100, 100), 412 (36, 48), 413 (13, 17), 414 (3, 4). Anal. Calcd for $C_{26}H_{35}OTi$: C, 75.9; H, 8.57. Found: C, 76.3; H, 8.59.

$Cp^*_2TiN(Et)Ph$. A mixture of Cp^*_2TiCl[16] (0.50 g, 1.4 mmol) and LiN(Et)Ph (0.20 g, 1.6 mmol) were suspended in 40 mL of diethyl ether. After the mixture was stirred for 3 h, the solvent was removed under reduced pressure. The black solid residue was suspended in 30 mL of hexane, and the mixture was filtered. The volume of the filtrate was reduced to *ca*. 3 mL. Cooling to −20 °C gave small black crystals (0.36 g, 58%). Mp = 174−181 °C. IR 2720 (w), 1370 (s), 1355 (w), 1340 (w), 1305 (s), 1280 (s), 1185 (m), 1135 (w), 1090 (m), 1020 (s), 980 (s), 850 (m), 775 (s), 745 (s), 695 (s), 635 (m), 535 (m), 485 (w), 450 (s), 420 (m), 405 (s), 370 (m), 345 (s) cm^{-1}. MS $(M)^+$ *m/z* (calc, found) 437 (13, 45), 438 (100, 100), 439 (39, 37), 440 (14, 13), 441 (2, 3). Anal. Calcd for $C_{28}H_{40}NTi$: C, 76.7; H, 9.19; N, 3.19. Found: C, 7.60; H, 9.28; N, 3.36.

$Cp^*_2TiN(Me)Ph$.[22] IR (not previously reported) 3075 (w), 3055 (w), 2720 (w), 2620 (w), 2570 (w), 1585 (s), 1555 (m), 1390 (s), 1190 (m), 1165 (m), 1050 (w), 1030 (m), 990 (s), 855 (w), 825 (s), 755 (s), 705 (m), 630 (w), 545 (w), 470 (w), 420 (m), 350 (m) cm^{-1}.

(38) Bercaw, J. E.; Marvich, R. H.; Bell, L. G.; Brintzinger, H. H. *J. Am. Chem. Soc*. **1972**, *94*, 1219.

(39) Daul, C.; Schlapfer, C. W.; Mohos, B.; Ammeter, J.; Gamp, E. *Comp. Phys. Commun*. **1981**, *21*, 385−395.

(40) Guenther, D.; Jaffe, A. *Horizon*; 1.3.0 ed.; Blue Star Software, Inc.: Honolulu, 1992.

X-ray Crystal Structure Determination for Cp^*_2TiF. Dark green crystals of the fluoride were grown by cooling a saturated hexane solution to −30 °C. A large, blocky single crystal was selected and a block-shaped piece measuring 0.30 × 0.40 × 0.45 mm was cut from one corner. The crystal was mounted on the end of a 0.4 mm diameter quartz capillary with a drop of Paratone N. The crystal was transferred to an Enraf-Nonius CAD-4 diffractometer[41] and cooled to −115 °C under a cold stream of nitrogen gas previously calibrated by a thermocouple placed in the sample position. Automatic peak search and indexing procedures indicated that the crystal possessed a primitive monoclinic cell and yielded the cell parameters. The cell parameters and data collection parameters are given in the supporting information.

The 5178 raw intensity data were converted to structure factor amplitudes and their esds by correction for scan speed, background, and Lorentz−polarization effects.[41,42] Inspection of the intensity standards showed a sudden intensity loss of 12% between hours 6 and 7. The data collected after hour 7 was corrected for a 12% loss in intensity. The 226 systematic absences (*h*,0,*l*) [*l* odd], (0,*k*,0) [*k* odd], the 191 redundant data (0,*k*,*l*) [*l* < 0], and the 225 data collected between hours 6 and 7 were then rejected yielding 4536 unique data of which 3188 possessed $F_o > 3\sigma(F_o)$. Azimuthal scan data showed a difference of $I_{min}/I_{max} = 0.81$; however, the absorption curves were asymmetric. No empirical absorption correction was applied. The systematic absences indicated that the space group was $P2_1/c$.

The cell volume indicated that 8 molecules were present in the unit cell. The titanium atom positions for the two independent molecules were obtained by solving the Patterson map with the program SHELXS86.[43] The remaining heavy atom positions were obtained by successive Fourier searches and cycles of refinement. The heavy atom structure was refined by standard least-squares techniques. The heavy atoms were refined isotropically, and the hydrogen positions were then calculated based upon idealized bonding geometry and assigned thermal parameters equal to 1.3 Å^2 larger than the carbon atom to which they were connected. A Gaussian absorption correction, DIFABS, was then used. The heavy atoms were then refined anisotropically. The fluorine atoms of both molecules appear to be either moving or disordered. A final difference Fourier map showed no additional atoms in the asymmetric unit. Examination of intermolecular close contacts (<3.5 Å) showed that the molecules were monomeric.

The final residuals for 397 variables refined against the 3188 unique data with $F_o > 3\sigma(F_o)$ were $R = 6.90\%$; $R_w = 9.11\%$, and GOF = 2.054. The *R* value for all data (including unobserved reflections) was 9.91%. The quantity minimized by the least-squares refinements was $w(|F_o| - |F_c|)^2$, where *w* is the weight given to a particular reflection. The *p*-factor,[44] used to reduce the weight of intense reflections, was set to 0.03 initially, but later changed to 0.07. The analytical form of the scattering factor tables for neutral atoms was used and all non-hydrogen scattering factors were corrected for both the real and imaginary components of anomalous dispersion.[45]

Inspection of the residuals ordered in the ranges of $\sin(\theta/\lambda)$, $|F_o|$, and parity and values of the individual indexes showed no trends. Five reflections had anomalously high values of $w\delta^2$, and were weighted to zero toward the end of the refinement. The largest positive and negative peaks in the final difference Fourier map have electron densities of 0.66 and −0.17 e$^-$/Å^3.

X-ray Crystal Structure Determination for $Cp^*_2TiN(Me)H$. Rose-colored crystals of the amide were grown by cooling a saturated hexane solution to −30 °C. A blade-shaped single crystal was selected and a roughly pyramidal chunk measuring 0.37 × 0.40 × 0.40 mm was cut from the tip. The crystal was mounted on the end of a 0.3 mm diameter glass capillary with a drop of Paratone N. The crystal was transferred to an Enraf-Nonius CAD-4 diffractometer[41] and cooled to −130 °C under a cold stream of nitrogen gas previously calibrated by a thermocouple placed in the sample position. The crystal was centered in the beam. Automatic peak search and indexing procedures indicated that the crystal possessed a primitive orthorhombic cell and yielded the cell parameters. The cell parameters and data collection parameters are given in the supporting information.

The 1514 raw intensity data were converted to structure factor amplitudes and their esds by correction for scan speed, background, and Lorentz−polarization effects.[41,42] Inspection of the intensity standards showed a smooth, slightly curved decay of 14% over the data collection. The data were corrected for a linear decay of 14%. The 20 systematic absences (*h*,0,0) [*h* odd], (0,*k*,0) [*k* odd], and (0,0,*l*) [*l* odd] were then rejected yielding 1494 unique data of which 1323 possessed $F_o > 3\sigma(F_o)$. Azimuthal scan data showed a difference of $I_{min}/I_{max} = 0.85$. An empirical absorption correction was applied. The systematic absences indicated that the space group was $P2_12_12_1$.

The cell volume indicated that 4 molecules were present in the unit cell. The titanium atom position was obtained by solving the Patterson map. Refinement on the titanium position led to the titanium becoming non-positive definite. However, a difference Fourier search yielded most of the other heavy atom positions. Refinement of these positions followed by a Fourier search yielded the remaining positions. The heavy atom structure was refined by standard least-squares and Fourier techniques. The heavy atoms were refined anisotropically, and a difference Fourier search showed that almost all of the hydrogen atoms could be located. The amide hydrogen was included in the refinement with an isotropic thermal parameter and it behaved normally. The other hydrogen positions were then calculated based upon idealized bonding geometry and assigned thermal parameters equal to 1.3 Å^2 larger than the carbon atom to which they were connected. The non-amide hydrogen positions were included in the structure factor calculations but not refined by least squares. At the end of the refinement, the enantiomer was changed, and the structure refined again. The refinement was very slightly worse, so the enantiomer was changed back to the original one, and the structure was rerefined. A final difference Fourier map showed no additional atoms in the asymmetric unit. Examination of intermolecular close contacts (<3.5 Å) showed that the molecule was a monomer.

The final residuals for 212 variables refined against the 1315 unique data with $F_o > 3\sigma(F_o)$ were $R = 4.83\%$, $R_w = 6.22\%$, and GOF = 2.04. The *R* value for all data (including unobserved reflections) was 5.58%. The quantity minimized by the least-squares refinements was $w(|F_o| - |F_c|)^2$, where *w* is the weight given to a particular reflection. The *p*-factor, used to reduce the weight of intense reflections, was set to 0.03 initially, but later changed to 0.05.[44] The analytical form of the scattering factor tables for neutral atoms were used and all non-hydrogen scattering factors were corrected for both the real and imaginary components of anomalous dispersion.[45]

Inspection of the residuals ordered in the ranges of $\sin(\theta/\lambda)$, $|F_o|$, and parity and values of the individual indexes showed no trends. Eight reflections had anomalously high values of $w\Delta^2$, and were weighted to zero toward the end of the refinement. The largest positive and negative

(41) Calculations were performed on a DEC Microvax II using locally modified Molen software operating under the Micro-VMS operating system.

(42) The data reduction formulas are

$$F_o^2 = \frac{\omega}{\mathrm{Lp}}(C - 2B) \qquad \sigma_o(F_o^2) = \frac{\omega}{\mathrm{Lp}}(C + 4B)^{1/2}$$

$$F_o\ (F_o^2)^{1/2} \qquad \omega_o(F) = [F_o^2 + \sigma_o(F_o^2)]^{1/2} - F_o$$

where *C* is the total count of the scan, *B* is the sum of the two background counts, ω is the scan speed used in deg/min, and

$$\frac{1}{\mathrm{Lp}} = \frac{\sin(2\theta)(1 + \cos^2(2\theta_m))}{1 + \cos^2(2\theta_m) - \sin^2(2\theta)}$$

is the correction for Lorentz and polarization effects for a reflection with scattering angle 2θ and radiation monochromatized with a 50% perfect single crystal monochrometer with scattering angle $2\theta_m$.

(43) Sheldrick, G. M. In *Crystallographic Computing 3*; Sheldrick, G. M., Goddard, R., Eds.; Oxford University Press: London, 1985; pp 175−189.

(44) $R = (\sum||F_o| - |F_c||)/\sum|F_o|$, $wR = [\sum(|F_o| - |F_c|)^2/\sum wF_o^2]^{1/2}$, and GOF = $[\sum(|F_o| - |F_c|)^2/(n_o - n_v)]^{1/2}$, where n_o is the number of observations and n_v is the number of variable parameters, and the weights were given by $w = 1/\sigma^2(F_o)$ and $\sigma(F_o^2) = [\sigma_o^2(F_o^2) + (pF^2)^2]^{1/2}$, where $\sigma^2(F_o)$ is calculated as above from $\sigma(F_o^2)$ and where *p* is the factor use to lower the weight of intense reflections.

(45) Cromer, D. T.; Waber, J. T. In *International Tables for X-Ray Crystallography*; Kynoch Press: Birmingham, England, 1974; Vol. IV.

peaks in the final difference Fourier map have electron densities of 0.43 and −0.58.

Acknowledgment. The authors would like to thank Dr. F. J. Hollander for assistance in the crystal structure analysis and Dr. Norman Edelstein for helpful discussion about EPR spectroscopy. W.L. would like to thank the National Science Foundation for a graduate fellowship. M.S. thanks the Miller Institute for a postdoctoral fellowship. This work was partially supported by the Director, Office of Energy Research, Office of Basic Energy Sciences, Chemical Sciences Division of the U.S. Department of Energy under Contract No. DE-AC03-76SF00098.

Supporting Information Available: Tables of bond distances and angles, tables of positional parameters, and tables of thermal parameters for $Cp^*_2TiN(H)Me$ and Cp^*_2TiF and a plot of the electronic spectra of the trivalent decamethyltitanocenes (17 pages). This material is contained in many libraries on microfiche, immediately follows this article in the microfilm version of the journal, can be ordered from the ACS, and can be downloaded from the Internet; see any current masthead page for ordering information and Internet access instructions. Tables of structure factors are available from the author.

JA953272O